Autoionization rates and energy levels of triplet nf, $v=1$ Rydberg states of H_2

M. D. Lindsay, A. W. Kam, J. R. Lawall, Ping Zhao, and F. M. Pipkin
Lyman Laboratory of Physics, Harvard University, Cambridge, Massachusetts 02138

E. E. Eyler
Department of Physics and Astronomy, The University of Delaware, Newark, Delaware 19716
(Received 21 November 1989)

We have measured the linewidths of 35 different triplet Rydberg states of the H_2 molecule with quantum numbers $n=10$–22, $L=3$, $v=1$, and $R=0$–4. An 18-eV electron beam excites a collimated H_2 beam to the metastable $c(2p)^3\Pi_u$ state. Stepwise excitation using two counterpropagating cw single-mode dye laser beams excites the metastable molecule first to an intermediate state [$(3d)^3\Sigma$ or $(3d)^3\Pi$] and then to a triplet nf Rydberg state. The linewidths for the nf Rydberg states give the autoionization rates, which agree satisfactorily with the polarizability–quadrupole-moment long-range interaction model. We also have measured the transition frequencies between these states to an accuracy of 0.002 cm^{-1}. We use these measurements to derive the ionization potential of the metastable triplet state to an accuracy of 0.020 cm^{-1} and the energy difference between the metastable and ground states of H_2 to an accuracy of 0.025 cm^{-1}.

I. INTRODUCTION

Although the energy levels of molecular Rydberg states are in many cases almost indistinguishable from those of their counterparts in simple atoms, their dynamical behavior can be completely different because of the presence of uniquely molecular decay pathways. For some time it has been realized that vibrational and rotational autoionization (also called preionization) can be important decay channels even for nonpenetrating Rydberg states of high n and L, since the electrostatic coupling of the molecular ion core to the distant Rydberg electron can couple the rovibronic and electronic motion.[1] For these nonpenetrating states both the energy levels and the autoionization rates can easily be predicted if the properties of the molecular ion core are known, as is the case for the simplest diatomic molecules and particularly for H_2. It is shown in Ref. 1 that the autoionization rates arising from these long-range couplings are typically much slower than those of the better-known example of strongly penetrating ns or np states,[2,3] but nevertheless are far faster than radiative decay. Until now a quantitative comparison of experiment and theory has not been possible, since accurate measurements of decay rates for high-L Rydberg states have been performed only for NO, where a careful theoretical treatment is still lacking.[4,5] In this paper we report accurate measurements of autoionization rates and energy levels for a variety of triplet nf Rydberg states of H_2 as a function of principal quantum number, rotational angular momentum, and total angular momentum excluding spin, and a detailed comparison with theoretical predictions.

Only since the 1970s has a systematic understanding of molecular Rydberg state structure and dynamics begun to emerge, but numerous pieces of the puzzle were assembled in a vast array of earlier studies. Experimental work on the Rydberg states of H_2 dates to the 1920s, when Richardson, Foster, and Davidson[6–8] measured the emission spectra of H_2 in a discharge and made many assignments of the transitions which occur between the low-lying states. Dieke[9,10] measured almost 100 000 emission lines of H_2, and assigned about half of them. From his compendium of lines Dieke derived energy levels for the non-Rydberg states which, when corrected for the then unknown singlet-triplet splitting,[11] are precise to better than 0.1 cm^{-1}. These very complete tables of transition energies were essential for planning the measurements reported in this paper. Lichten and co-workers,[12,13] and Miller, Freund, and co-workers[11,14,15] have reported measurements of relatively low-lying states of H_2, with $n=2$ or 3, which provide a detailed description of the fine and hyperfine structure of these states. In 1969 Jungen and Miescher[16] studied the absorption spectrum of NO and assigned numerous $4f$ and $5f$ levels. Their analysis included a theoretical description of the interaction between the nonpenetrating Rydberg electron and the polarizability, dipole, and quadrupole moments of the NO^+ core. Using the model of Ref. 16, Herzberg and Jungen[17] identified the $5g$-$4f$ transitions of H_2 and D_2, as well as some $4f$-$3d$ transitions. Eyler and Pipkin's formulation of the quadrupole-polarizability model[1,18,19] used in this paper is similar, but is derived in Hund's case d, where the Hamiltonian is nearly diagonal. Sturrus, Hessels, Lundeen, and co-workers[20] extended the polarizability and multipole moment long-range model of the molecular core, and measured the $n=10$ manifold of H_2, with $L=3$–8, using both laser and microwave spectroscopy. An important idea developed in Ref. 16 is the use of the Rydberg electron as a precise "probe" of the positive ion molecular core, allowing properties of the core such as its quadrupole moment to be derived from analysis of the Rydberg spectrum. In this paper we use the inverse pro-

cess; we start with calculated H_2^+ molecular core constants,[21–23] and derive from them the autoionization rates and energy levels.

The model of a vibrationally and rotationally excited core with time-varying multipole fields that cause ionization of the Rydberg electron was used by Russek, Patterson, and Becker[24] to estimate autoionization rates of H_2 and HD, principally for the low-L states for which the method unfortunately is not appropriate because of strong core penetration.

Multichannel quantum-defect theory[25,26] (MQDT) has been used to calculate the autoionization rates and perturbed energy levels of Rydberg H_2.[27] Although the theory is general, the most detailed calculations and measurements have been for the singlet np states. The core penetration of the Rydberg electron for these states is much larger than for the nf states which we have studied. The interaction between the np Rydberg electron and the core is stronger, and the energy-level perturbations and autoionization rates are larger than for nf Rydberg electrons. For example, Dehmer and Chupka[2,3] observed linewidths corresponding to autoionization rates for np states on the order of 10^{12} s^{-1}, which are about 1000 times larger than the typical rates we observe for the nf states reported in this paper. For states which have large core penetration, such as the np states mentioned above, it is necessary to use MQDT to calculate linewidths; for states with weak core penetration, one can use either MQDT or the long-range model which utilizes the interaction between the Rydberg electron and the quadrupole moment and polarizability of the H_2^+ core. Jungen *et al.*[28] have recently used MQDT to calculate the positions and microwave intervals between 10g, 10h, and 10i Rydberg states. These states are somewhat less penetrating than the nf states we studied. Jungen *et al.* compared their theoretical results with the calculations of the same intervals by Lundeen and co-workers,[20] who used the apparently quite different long-range interaction model. The two approaches agree very well, and also agree with measurements of the intervals.[20,28] One may conclude that for high-L Rydberg states of H_2, the results of MQDT and the long-range interaction model are equivalent.

The above paragraphs are by no means a complete list of all the work that has been done on Rydberg states of H_2. Some reviews are given by Richardson,[8] Herzberg,[29] Dieke,[10] Krauss,[30] Sharp,[31] (shows detailed potential curves for H_2), Herzberg,[32] Bishop and Cheung,[33] and Freund.[34]

Eyler, Pipkin, and co-workers[1,18,35–38] have made extensive measurements and calculations on Rydberg H_2. This paper describes an extension of this work. We have measured the natural linewidths and absolute energy levels of 35 triplet nf Rydberg states of H_2 with a range of quantum numbers $n=10$–22, $L=3$, $v=1$, and $R=0$–4. This paper reports the first measurements of autoionization rates of nonpenetrating Rydberg states of H_2 and thus the first quantitative test of the theory in Ref. 1. It also reports measurements of the absolute energy levels of the Rydberg states relative to the metastable $c(2p)^3\Pi_u$ state that are five times more precise than previous work.

TABLE I. Rovibrational levels of H_2^+ core, with respect to the $v=0$, $R=0$ level, used in analysis of data. These values are taken from the calculation of Bishop and Cheung (Ref. 22). $E(1,3)$ is an extrapolation based on the three other values, compared with Hunter, Yau, and Pritchard's values (Ref. 39).

$E(v,R)$	Energy level (cm^{-1})
$E(1,0)$	2191.1273(20)
$E(1,1)$	2246.2939(20)
$E(1,2)$	2356.1823(20)
$E(1,3)$	2519.9298(30)

Using the long-range interaction model together with calculations of the vibrational and rotational spacings of the core[22] we derive a measurement of the ionization potential of the metastable $c(2p)^3\Pi_u$ state from which we do our optical excitations. The recent measurement by McCormack *et al.*[38] of the ionization potential of H_2 from the ground state, combined with our data, yields a very precise value of the interval between the (singlet) ground state of H_2 and the $c(2p)^3\Pi_u$ metastable state. Thus the energy levels of the triplet and singlet manifolds of H_2 can be linked to each other with high precision.

Bishop and Cheung have done precise calculations of H_2^+ polarizabilities as a function of internuclear separation.[21] We use the results of Karl *et al.*[23] for the quadrupole moments of H_2^+. We use Bishop and Cheung's values for the rovibrational spacings[22] of the H_2^+ core, which are accurate to 0.002 cm^{-1} and take into account radiative, relativistic, and nonadiabatic effects. The specific values of the rovibrational spacings $E(v,R)$ are listed in Table I. Hunter, Yau, and Pritchard,[39] and Hunt, Poll, and Wolniewicz[40] also have compiled tables of these values.

This paper is divided into five major sections. Section II summarizes the theory of the long-range interaction of the H_2^+ core and the Rydberg electron and describes the structure of the states of interest. The apparatus and experimental procedure are described in detail in Sec. III. Section IV describes the data analysis and compares the results with theory. Section V is the conclusion.

II. NOTATION AND SUMMARY OF THEORY

This paper follows the notation used by Hougen.[41] The $2p$ and $3d$ states are labeled according to Hund's case-b notation, shown schematically in Fig. 1(a), where Λ represents the projection of the electronic orbital angular momentum on the internuclear axes; **N** the total angular momentum exclusive of spin; and **S** the total electron spin angular momentum. As the average distance between the outer electron and the core increases, the orbital angular momentum **L** of the outer electron decouples from the nuclear axis and Λ is no longer a good quantum number. Case-d coupling, shown in Fig. 1(b), is used to describe the nf Rydberg states. The core rotation is called **R**; the alternative notation $\mathbf{N}^+$ is also widely used. In case d the total angular momentum excluding

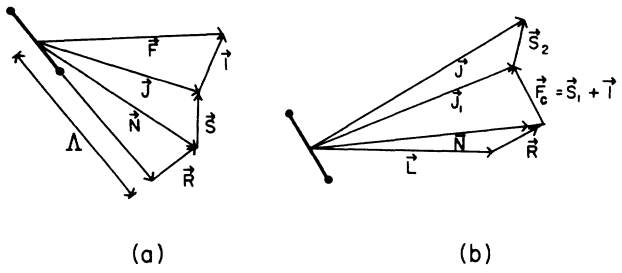

FIG. 1. The angular momentum coupling diagrams for the states of interest. (a) The lower energy states ($2p$ and $3d$) are described by Hund's case b. (b) The Rydberg states are described by a special case of Hund's case d, in which the total spin $\mathbf{S}$ is not a good quantum number. $\mathbf{S}_1$, the spin of the core electron, first couples with the total nuclear spin to form $\mathbf{F}_c$. $\mathbf{J}_1=\mathbf{N}+\mathbf{F}_c$, and then the spin of the outer electron $\mathbf{S}_2$ couples to $\mathbf{J}_1$ to form $\mathbf{J}$. (see Ref. 20.)

spin is $\mathbf{N}=\mathbf{R}+\mathbf{L}$. The transition from case b to case d depends both on n and L. For example, $2p$ states are largely case b, $3d$ states are intermediate, and nf states are largely case d for n as small as 4. Λ is not a particularly good quantum number for $3d$ triplet states, and a $3d$ state labeled, e.g., Π may have large admixtures of Σ and/or Δ character. For these states we use the level designations of Dieke, given in Crosswhite's compilation.[9]

In the simplest version of the long-range interaction theory[1,18,20] of the energy levels and autoionization rates, the Rydberg states are described by Hund's case-d wave functions. Electronic and nuclear spin are ignored in this model. The interaction Hamiltonian $\mathcal{H}'$ of the Rydberg electron with the core ion is approximated by the first nonzero[42] term of a multipole expansion of the Coulomb interaction, the quadrupole term, together with the lowest-order polarizability,

$$\mathcal{H}'=\mathcal{H}_{\text{quad}}+\mathcal{H}_{\text{pol}} .$$

The wave functions of the case-d states and the matrix elements of this perturbation are given explicitly in Ref. 18. The energy levels of the Rydberg states are given by H atom energy levels, corrected by the above perturbation, calculated to second order.[18,36] Autoionization rates are given by Fermi's "golden rule," which uses the above perturbation to link a quasistationary Rydberg state and a continuum state.[1,24] It can be shown that for isolated states the autoionization rate scales as n^{-3}. This has been experimentally verified for singlet np Rydberg states of H_2.[2,3] We have used computer programs to perform the necessary numerical integrations and calculate the energy levels and autoionization rates of specific Rydberg levels.

The levels of H_2 we measure are split by the spin in-

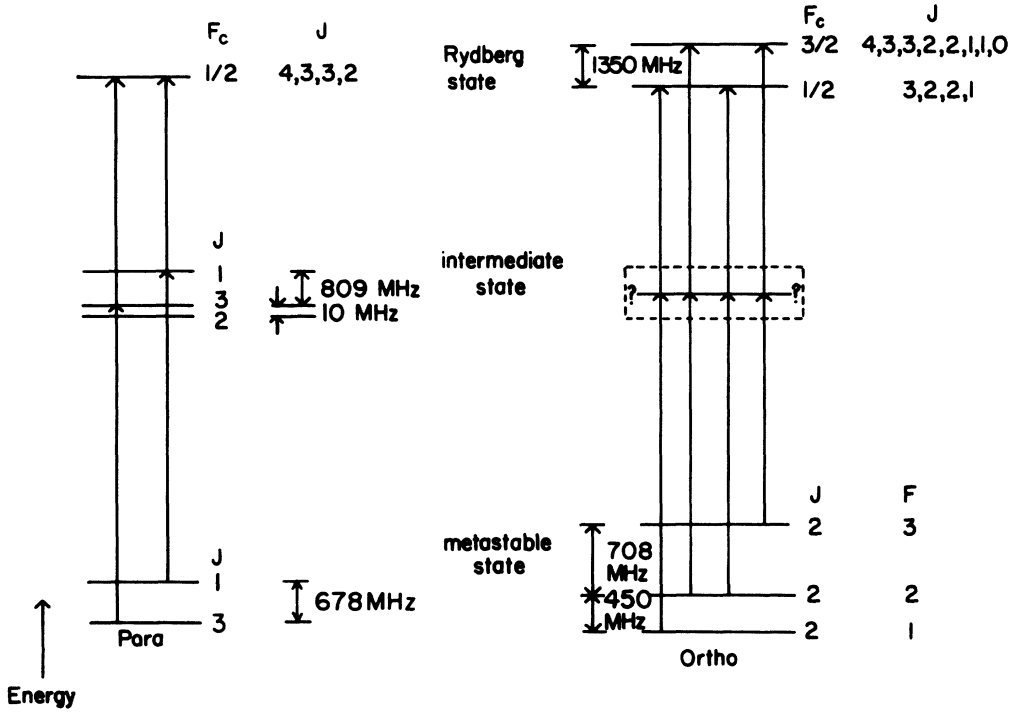

FIG. 2. Excitation scheme, showing spin splitting of levels which leads to resolved structure of the lines observed. The para-H_2 transition is nf, $v=1,R=0,N=3\leftarrow$intermediate$\leftarrow(2p)^3\Pi_u,v=1,N=2,J=3$, and the ortho-$H_2$ transition is nf, $v=1,R=1,N=2\leftarrow$intermediate$\leftarrow(2p)^3\Pi_u,v=1,N=1,J=2$. Schemes for other transitions are similar. For para-H_2, there is much less structure, since $I=0$, thus $F_c=\frac{1}{2}$ only. Vertical lines indicate resolved transitions. This diagram is not to scale vertically.

teractions. Transitions to different spin levels differ in frequency by up to 2000 MHz, significantly larger than the resolution of our measurements. The spin structure of the $2p$ metastable states and the $3d$ states has been studied extensively.[13,14] The $2p$ spin states are identified by the usual J and F ($J=F$ in para-H_2). For Rydberg spin states, we use the notation of Lundeen and coworkers,[20] which they developed in their experimental and theoretical work on the spin structure of the Rydberg states. The splitting of Rydberg states into levels is due in part to the "magnetic dipole hyperfine" interaction in which the core electron spin $\mathbf{S}_1$ couples to the nuclear spin $\mathbf{I}$ to form $\mathbf{F}_c$. [See Fig. 1(b) and Ref. 20.]

In para-H_2 the metastable $2p$ state is split by interactions with electronic spin into levels of various J. For transitions between para states, we measure transitions from the level of maximum J of the $2p$ state, to the single possible value of F_c of the Rydberg state. Since there are two intermediate levels very close in energy excited simultaneously by the first laser (due to the Doppler width of the molecular beam), a given final Rydberg state sublevel is excited by two different frequency settings of the second laser. The transition frequencies reported here are for frequencies of transitions into and out of the intermediate level of maximum J.

In ortho-H_2 the metastable $2p$ state is split by interactions with electronic and nuclear spin into levels of various J and F. For ortho states, transitions occur from a given J level, with its three F sublevels ($F=J-1,J,J+1$), to the two possible values of F_c of the Rydberg state. Our reported transition frequencies are for transitions from the $2p$ level of maximum J and maximum F, through the intermediate level of maximum J, to the Rydberg level of maximum F_c. The structure of the intermediate ortho state is not well known, but apparently only one sublevel participates as the intermediate state. Figure 2 shows a sketch of the relevant spin structure for the initial, intermediate, and final states of typical para- and ortho-H_2 transitions. Only the levels used in the measurements reported here are shown.

III. EXPERIMENTAL METHOD

The excitation scheme and potential curves of the H_2 states of interest are shown in Fig. 3. The Rydberg states, if they had minimum core energy ($v=0$ and $R=0$ for para-H_2, $R=1$ for ortho-H_2), would have energies slightly less than the ionization energy. Our excitation scheme produces Rydberg states with one or more vibrational and/or rotational quanta in the core, which gives the total system an energy above the ionization energy, allowing autoionization.

The apparatus is a modification of that used in earlier laser-molecular-beam experiments which studied triplet states of H_2.[18,19,35,36] We start with high-purity H_2 gas (grade 5 from Airco Company) at room temperature, fed through a needle valve to the electron bombarder. This bombarder is designed to produce the maximum number of metastable H_2 molecules in the thermal effusive beam. The present bombarder[19] is very similar to one first used

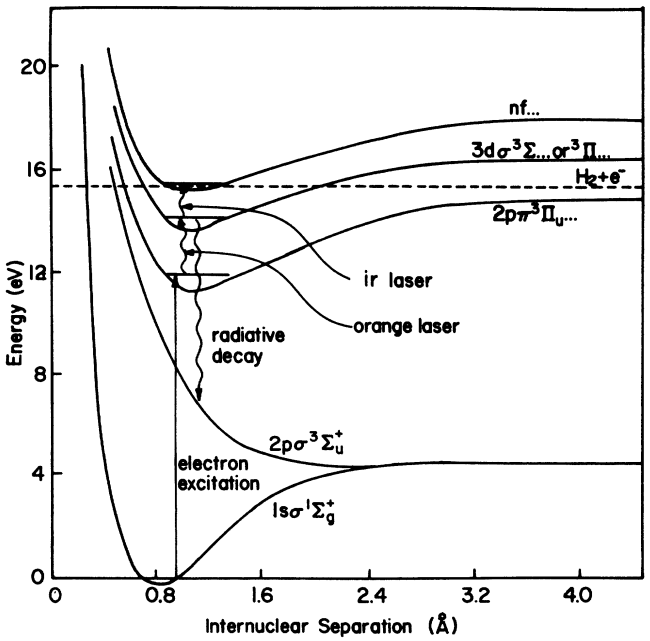

FIG. 3. Energy-level diagram for H_2 showing excitation scheme. The $nf\ldots$ state decays to $H_2^+ + e^-$. The ellipses indicate all the other quantum numbers necessary to fully identify the state.

by Lichten.[12] Figure 4 shows a schematic of the electron bombarder, which is located in an oil diffusion-pumped vacuum chamber. H_2 gas travels through a narrow (0.01-cm) slit in a solid Cu rod into the vacuum chamber.[43] The slit is parallel to a strong magnetic field (0.4 T) produced by permanent magnets. A glowing tungsten filament, aligned with the slit, is set at -18 V relative to the Cu rod and slit. The magnetic field collimates the emitted electrons into a sheet which passes into the slit and bombards the ground-state H_2. Thus the singlet ground-state molecules are excited into many states, including the $c(2p)^3\Pi_u$ $v=1$ metastable levels used as the lower levels for our optical excitations. Excited molecules in the triplet metastable state reach the laser-beam interaction region, where they are excited to triplet Rydberg states. Other excited states are not resonant with the lasers. We estimate that the electron bombarder excites about 1 in 10^6 of the molecules to a given sublevel of the metastable state. With H_2 gas flowing to the apparatus, the pressure in the chamber containing the electron bombarder is about 5×10^{-5} Torr. The heater current of the tungsten filament is regulated so that the emission current of the filament remains constant, and hence the flux of metastable H_2 in the molecular beam remains constant.

The beam of metastable H_2 travels 20 cm to a 5-mm-wide slit, giving a collimation ratio of 40. Just beyond the collimating slit is the laser interaction region, pumped by another oil diffusion pump to about 2×10^{-6} Torr with the gas on. Using the geometric size of the molecule as an upper limit of the cross section, the mean

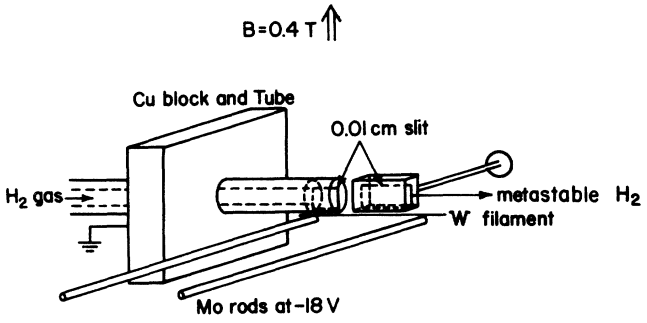

FIG. 4. Electron bombarder, which produces a beam of metastable H_2 molecules in the $c(2p)^3\Pi_u$ state.

free path at this pressure is ~ 5 mm even for our largest ($n=22$) Rydberg molecules. The entire laser excitation and autoionization takes place in less than 50 ns, much less than the mean time between collisions of ~ 10 μs, so the H_2 molecules do not collide while being measured. We repeatedly sprayed the entire inside of the vacuum chamber with an alcohol suspension of powdered graphite (Aerodag G from Acheson Colloids Company) to give a conductive coating that helped to minimize stray static electric fields. Without the graphite coating, static fields built up within 5 s to at least 10 V/cm within 1 cm of some surfaces. Two plates (3×7 cm), each with a hole covered by a mesh in the center, were 5 mm above and below the laser-molecular-beam interaction region, as shown in Fig. 5. These plates (also coated with graphite) were attached to insulating mounts and electrically connected to the outside of the chamber. For data taking we shorted and grounded the plates, and applied fields only to test how the lines were affected. The magnetic field in the laser-molecular-beam interaction region was solely due to the earth's field; effects of the permanent magnets 20 cm away were negligible. This 0.5-G field had no significant effect on the states measured.

The laser beams came from two Coherent single-mode cw dye lasers: models 599 and 699. The model 599, a standing-wave laser, used rhodamine 6G (the "orange" laser); and the model 699, a ring laser, used styryl 9M dye (the "ir" laser), covering a range from about 800 to 850 nm. Both were locked to the peak of a cavity mode using a piezo-mounted thick étalon in the cavity, as supplied by Coherent. We estimate the linewidth of each of these lasers to be 20 MHz. The beams were carefully aligned to be collinear, counterpropagating, and at exact right angles to the molecular beam. They were focused at the interaction region with 20-cm focal length cylindrical lenses. A diagram of the optical setup is in Fig. 6.

The orange laser, when set to the peak of the intermediate transition, was locked to a thermally stabilized

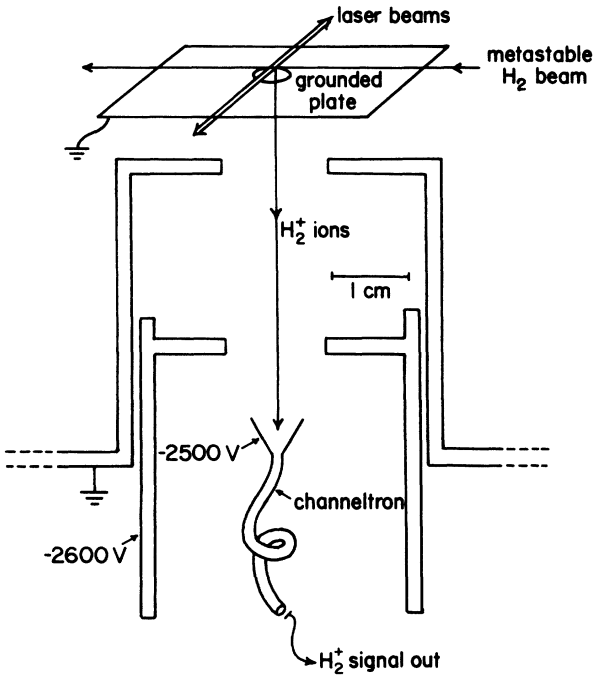

FIG. 5. Schematic of H_2^+ detector. The lower part of this figure is a scale cross-sectional view of the channeltron holder and electrostatic lens. It has axial symmetry about the H_2^+-ion path. The upper part of the figure is a perspective drawing of the laser-molecular-beam interaction region, with the top grounded shielding plate removed. The laser beams and plates are perpendicular to the plane of the paper.

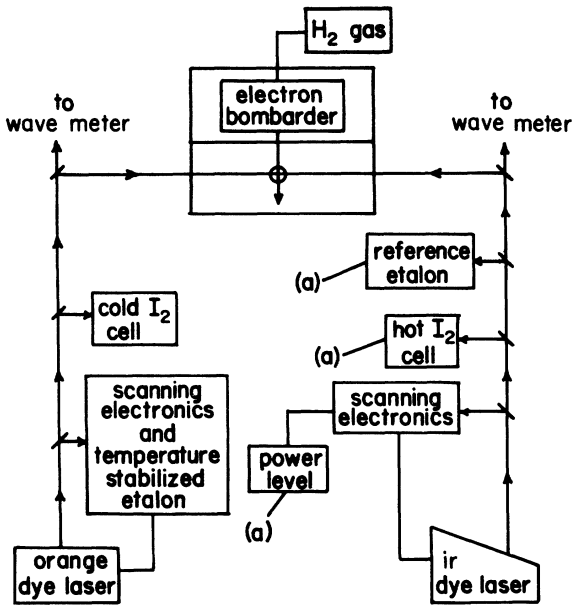

FIG. 6. Apparatus for two-laser spectroscopy of H_2. The (a)'s are the three channels of data recorded while the orange laser is set to an intermediate transition and the ir laser is scanned over a Rydberg transition. The fourth data channel is the count rate of the channeltron H_2^+ ion detector, which monitors excitation to the autoionizing Rydberg states. The H_2^+ detector is placed under the point where the laser beams and molecular beam cross. A uv-sensitive PMT is placed over the same point to monitor excitation to the intermediate state. The reference étalon gives frequency markers spaced at 297.75 MHz.

external reference etalon (Burleigh model CFT-25P ir). We checked regularly to see if this laser was still on the peak of the intermediate transition, and reset it as needed. Once the orange laser system had warmed up, it did not need to be reset for many hours.

A galvo-mounted intracavity plate in the ir laser, controlled by a circuit designed to produce scanning at a constant rate, was tilted slightly to tune the frequency of the laser across the molecular transitions. We scanned the ir laser through the transition at 7, 15, or 30 MHz/s and sampled the data at 3, 5, or 10 samples/s, respectively. While scanning, we sent a portion of the ir beam through a sealed étalon with a Cervit spacer of length 50.329 34±0.000 13 cm and a finess of about 3. The fringe spacing of 297.749 MHz calibrated the width measurements. If the ir laser jumped a cavity mode, the regular pattern of fringes was clearly disrupted, and the scan was discarded.

The absolute frequencies of the lasers were measured in two ways: with iodine cells or with a wave meter. For the orange laser, we used a room-temperature I_2 cell consisting of I_2 crystals in a glass vacuum cell. The single-mode laser light traveled down the length of the cell and a photodiode received the fluorescence emitted at right angles. We compared the resulting plethora of lines to the I_2 atlas compiled by Gerstenkorn and Luc[44] and matched the lines unambiguously. As the laser scanned, the output of the photodiode looked similar to the spectra in the atlas taken with a very different Fourier spectrometer. For the ir laser, we used a hot I_2 cell consisting of an evacuated fused silica tube held at 900 °C with I_2 vapor inside. The ir beam traversed the I_2 cell directly onto a simple photodiode. Again, the photodiode output looked similar to the lines in the I_2 atlas by Gerstenkorn, Verges, and Chevillard.[45]

A homemade Michelson traveling-arm interferometer (λ meter, or wave meter)[46,47] was used for precise absolute frequency measurements. We measured both the orange laser and the ir laser separately while they were each set to the peaks of their respective transitions. The reference laser for the wave meter was a Zeeman-stabilized He-Ne laser.[48] We calibrated the He-Ne laser tube by beating it with the output of a National Institute of Standards and Technology I_2-stabilized He-Ne laser and by observing the beat note with a fast photodiode and a spectrum analyzer. The He-Ne laser's frequency was measured to be 473 612 260±10 MHz, which is 15 798.0045(3) cm^{-1}. Using the wave meter we measured the frequency of each transition at least 50 times and made (small) corrections for variations in room temperature and pressure. We also measured the absolute frequencies of some H_2 transitions by interpolating between I_2 lines from the atlases.[44,45] Within the quoted uncertainties of the I_2 atlases, these two methods agreed.

The orange laser excited the $2p$ metastable molecules to the $3d$ levels, which decay to the $b\,(2p)^3\Sigma_u^+$ dissociative state by emitting a uv photon with energy in the range 6–8 eV. To detect these photons and monitor the excitation to the intermediate state, we placed a broadband vacuum uv photomultiplier tube (PMT) (EMI G24H314LF) about 2 cm away from the laser-molecular-beam interaction region, and 1 cm above the wire mesh of one of the graphite-coated plates. This PMT was only very slightly sensitive to visible light and as long as the lasers were aligned properly so that they illuminated only the molecular beam, stray laser photons contributed nothing to the background. Using only the orange laser, we did high-resolution spectroscopy of the $3d \leftarrow 2p$ transitions. A typical scan over about 1 cm^{-1} is shown in Fig. 7. To obtain a double-resonance spectrum of the Rydberg states, we set the orange laser to the peak of a selected $3d \leftarrow 2p$ transition (on the $J'_{max} \leftarrow J''_{max}$ component) and scanned the ir laser. For these intermediate transitions, there were about 4000 counts/s of background, presumably due to stray uv light emitted by metastable H_2 molecules. The intermediate transition provided about 2500 counts/s of signal at its peak.

The ir laser excited the molecules in the $(3d)^3\Sigma$ or $(3d)^3\Pi$ states up to the Rydberg states. The H_2^+ ion fragment from autoionization of the Rydberg state was detected. This detector was first configured to observe electrons,[36] but we found that the positive-ion background was an order of magnitude smaller, while the H_2^+ signal from a transition was only slightly smaller than the electron signal. Many of the weaker lines presented in this paper would have been too weak to distinguish from the noise background if electron detection had been used. The H_2^+ autoionization fragments passed through the grid of the other plate into a simple electrostatic lens and finally to a channeltron detector (Galileo 4730). The H_2^+ detector is shown in Fig. 5. The background count rate was about 1000 counts/s. For the strongest transitions measured and for relatively high ir laser power of 200 mW, our largest signals were 20 000 counts/s. Most lines were weaker; the weakest had a signal size of about 200 counts/s, which was still clearly visible above the background. Typical scans of transitions to Rydberg states are shown in Figs. 8(a)–8(c).

Line identifications were easily made by correspon-

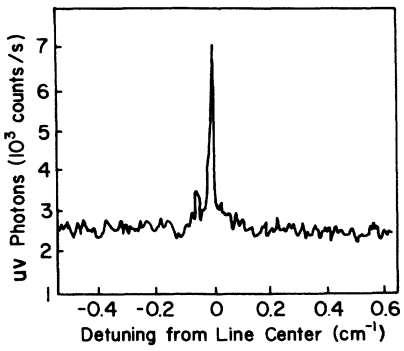

FIG. 7. The line profile acquired while scanning the orange laser over the $(3d)^3\Sigma, v=1, N=1 \leftarrow (2p)^3\Pi_u, v=1, N=1$ transition. The peak is the $J'=2 \leftarrow J''=2$ branch. The small side peaks within 0.08 cm^{-1} of the main peak are due to J splitting of the intermediate state. Other intermediate transitions look similar.

dence with predicted energies. The spectra taken with the orange laser alone, or with both lasers, were quite sparse. Lines were separated on average by 10 000 times their width, and in the case of the closest sets of lines, by no less than 0.3 cm^{-1}.

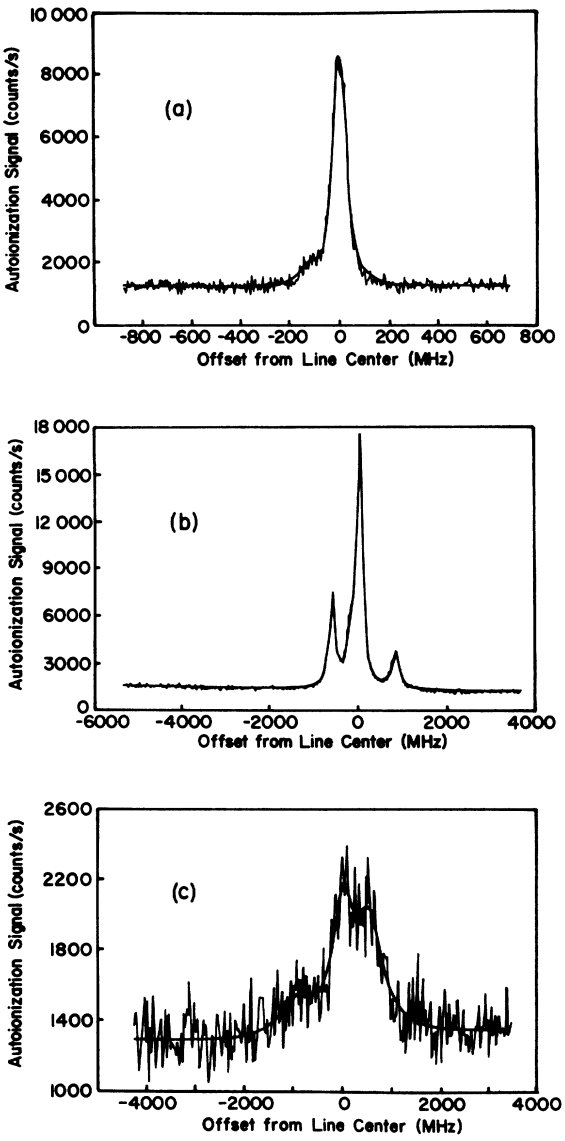

FIG. 8. Typical line profiles acquired while scanning the ir laser over transitions from the intermediate states to the Rydberg states. The smooth line is the sum-of-Lorentzians fit, as described in Sec. IV A of the text. (a) is the transition $20f\,v=1\,R=2\,N=4\leftarrow(3d)^3\Pi\,v=1\,N=3\,J=4$. (b) is the transition $14f\,v=1\,R=1\,N=2\leftarrow(3d)^3\Sigma\,v=1\,N=1\,J=2$, and has relatively large signal-to-noise ratio (S/N). (c) is the transition $11f\,v=1\,R=3\,N=0\leftarrow(3d)^3\Sigma\,v=1\,N=1\,J=2$, and has relatively small S/N. The Rydberg transitions measured all had a two, three, or four Lorentzian form as above, and all had a S/N in the range shown above. The S/N is not correlated with number-of-Lorentzians line shape. For (a) and (b) the frequency of the laser increases from left to right; for (c) the frequency increases from right to left.

While the orange laser was fixed to the intermediate transition and the ir laser scanned, we recorded with a computer four data channels: the output of the channeltron, the fringes of the 50-cm Cervit étalon, the ir I_2 lines from the hot I_2 cell, and the laser power level of the ir laser. As the ir laser was scanned over the width of an H_2 line (at most 1000 MHz or 0.03 cm^{-1}) the power changed by as much as 3%. Since the signal was proportional to ir laser power, this distorted the line shapes slightly. We normalized the data using the ir laser power to correct for this distortion. Throughout the experiment we used normal H_2 which consists of 75% ortho-H_2 and 25% para-H_2. By using an enriched source of para-H_2, one could increase the signal-to-noise ratio of the para-H_2 lines. However, these particular $v=1$ lines were strong enough that this was not necessary.

IV. DATA ANALYSIS AND RESULTS

A. Widths

Each scan over a transition to a Rydberg state was typically represented by a set of about 1000 samples. We fit these scans to a function that is the sum of the appropriate number of Lorentzians plus a polynomial background, using the Levenberg-Marquardt method.[49] The fit function was

$$y_{\rm fit}(\nu)=a_1+a_2\nu+a_3\nu^2+\sum_{i=1}^{n}\frac{h_i(\Gamma_i/2)^2}{(\nu-\nu_{0i})^2+(\Gamma_i/2)^2}\,,\qquad n=2,3,\text{ or }4 \quad (1)$$

where a_1 is the constant background, a_2 and a_3 are the coefficients of the linear and parabolic background, and h_i, ν_{0i}, and Γ_i are the height, center, and full width at half-maximum of the ith Lorentzian. Each parameter varied freely in the fit, although excluding the $a_3\nu^2$ term has no statistically significant effect on the width parameters. Figures 8(a)–8(c) show paradigms of two, four, and three Lorentzian line shapes, with the fits shown superposed on the experimental spectra.

The line shapes are pure Lorentzians rather than Fano interference profiles, since the dipole matrix element for $nf\leftarrow 3d$ excitation is much larger than that for direct excitation to the continuum.[1] The structure of the lines arises from the fine and hyperfine structure resulting from the interaction of the magnetic moment of the electrons and nuclei with the rotational magnetic moment, the orbital magnetic field, and with each other. One expects the autoionization rates will depend primarily on n, L, v, R, and N, and not on the spin level. After adding all the spins to an $|n,L,v,R,N\rangle$ Rydberg state, twelve different spin levels of ortho-H_2 and four different spin levels of para-H_2 are obtained. Some of the splittings are large ($\approx$1000 MHz), which makes them easy to resolve. In this case the method of fitting to multiple Lorentzians extracts the true width. However, some of the splittings are in the range 0–20 MHz, which is at or below our system resolution. Most of the splitting that is in this range is due to the H_2^+ core and does not depend on n. This

gives a lower limit on the measured linewidth as n increases, since the width due to autoionization goes as n^{-3}. These unresolved splittings could distort the data by making a line look wider than what would occur in the ideal case of no spin splitting. The unresolved transitions are to the Rydberg sublevels of various J [which already includes I, as defined in Fig. 1(b)]. By analogy with the relative line strengths of transitions from different spin sublevels of the $2p$ state, we expect that the transition to the sublevel of maximum J will be at least three times more intense than transitions to any other J sublevels. Thus, for the unresolved sublevels of a resolved line, one sublevel will dominate the others. The width of the superposition of unresolved sublevels will be nearly the same as the width of the dominant transition to the single J sublevel having $J=J_{\max}$. If there were any significant deviations from the situation described above, the resolved components would have noticeably non-Lorentzian shapes; in particular, the wings of the measured line shape would be too broad and probably asymmetric. All our lines did, in fact, have a nearly undistorted Lorentzian shape, with the fit giving a reduced χ^2 of 2–3, if one assumes that the only source of noise is shot noise. When fitting a line shape we allowed the widths of each resolved component to vary independently during the fit. The near equality of the obtained widths (within about 15%) confirmed our expectation that unresolved spin splitting does not introduce spurious broadening, since one would expect this broadening to be different for each resolved component. In the case of the three and four component ortho-H_2 lines, the smallest outlying component was consistently 20% wider than the other two or three components. Apparently this broadening was caused by the unresolved hyperfine structure as described above. This component was not used in determining the reported rates. Since para-H_2 has less unresolved structure, our results for it are less susceptible to possible systematic broadening.

We obtained a minimum of at least three good scans and fits for each line reported, and most lines were examined at least ten times over several days to make sure the widths were consistent. The measured width of a line varied up to 20% from scan to scan. Slight momentary irregularities in the scanning rate of the ir laser and random differences in the noise background could cause the line to have slightly wider or narrower shoulders. The width for each component of a line is simply the average of the individual values we measured. The raw result for an ortho-H_2 line is an average of the widths of the two most narrow and bright components, since they are apparently less broadened by spin splittings. The raw result for a para-H_2 line is the width of the bright component. The measured line shape is actually a Voigt profile (or a sum of Voigt profiles each of which has similar width parameters). When the width of the Lorentzian component of a Voigt profile is much greater than the width of the Gaussian component, fitting the Voigt profile to a pure Lorentzian profile and then subtracting in quadrature the width of the Gaussian component gives the true Lorentzian width. We measured the residual Doppler width of our two laser-molecular-beam system to be 60 ± 10 MHz at 810 nm. Accordingly, we subtracted in quadrature 60 MHz from all raw widths greater than 120 MHz, to obtain the final result. When the widths of the Gaussian and Lorentzian components of a Voigt profile are about the same, no simple rule applies for deconvolving the original Lorentzian width. We generated on a computer Voigt profiles with a range of original Lorentzian widths and a fixed Gaussian width of 60 MHz. We then fit pure Lorentzians to these simulations, and obtained a table of fitted Lorentzian widths versus original Lorentzian widths. The fitted Lorentzian widths less than 120 MHz were transformed into the true Lorentzian widths using this table. The uncertainties of the widths are determined by the standard deviation of all widths for all the scans taken of a line, added in quadrature to the 10 MHz uncertainty of the system Doppler width. Our minimum measurable width was approximately 30 MHz, and since the rate is $2\pi\times$(width), our method can detect autoionization that occurs at a rate less than $10^8\ s^{-1}$, but we cannot accurately measure the rate for such slow decays. We only know that it is less than or equal to $10^8\ s^{-1}$ if we see a $\sim$30-MHz-wide line.

The intensity of the ir laser at the interaction region was approximately 10 W/cm^2. The dependence of the widths on ir laser power was examined using two different methods: (i) we reduced the ir laser power by a factor x ($x=2-10$), and the signal size of the transition consistently decreased by the same factor of x, within an uncertainty given by the square root of the signal size (count rate); this indicated the transitions were unsaturated, and (ii) we directly measured the widths of the lines at reduced ir power by taking scans and fitting them. With the ir laser power at 40 mW instead of the usual 80–200 mW, there was no change in the width of the lines within the $\sim$20 MHz uncertainty. In contrast, the intermediate-state transitions excited from the metastable state by the orange laser were completely saturated. A reduction of the power of this laser by a factor of 2 also did not change the width of the ir transitions to the Rydberg states.

Static electric fields were applied to the laser-molecular-beam interaction region to test whether stray fields might spuriously broaden the lines. We applied fields which ranged in value from 1 mV/cm to 1000 V/cm. At high fields, within the range from 100 to 1000 V/cm, the lines were broadened, distorted, and shifted by as much as 2 cm^{-1}. Above 500 V/cm, the weak lines disappeared and the strongest lines were barely detectable. At lower fields, broadening and shifting were not observed below an n-dependent electric field threshold. This threshold field was about 10 V/cm for $n=10$ and about 1 V/cm for $n=22$. We estimate that the stray electric field in our graphite-coated interaction region was less than 10 mV/cm for all data taking; thus the lines were not broadened or shifted by stray electric fields.

Table II summarizes the measured widths and the autoionization rates for the nf, $v=1$ triplet Rydberg states studied in this experiment, and shows the theoretically predicted widths, along with the ratios and differences of measured widths and theoretical widths. Theory and experiment agree satisfactorily within the limits of experi-

mental uncertainty. For fixed values of L, v, R, and N, the general dependence of decay rate on n^{-3} is clear. Figures 9 and 10 show decay widths scaled by multiplying by n^3 on the vertical axis, versus n on the horizontal axis. Figure 9 show the para series $n=11-20$, $L=3$, $R=0$, and $N=3$. Figure 10 shows the ortho series $n=11-21$, $L=3$, $R=1$, and $N=2$. The nearly flat line in these two figures passes through the scaled theoretical width predictions for these states. Since the theory predicts that the autoionization rates should go as n^{-3}, the scaled theory and measurements should be independent of n. Additionally, certain pairs of transitions isolate the dependence on R and N. For example, the pair of states $11f$, $R=2$, $N=2$ and $11f$, $R=1$, $N=2$ differ in width, and therefore in autoionization rate, by a factor of 2.36(33), in agreement with the theoretical value 2.06, due solely to their difference in R. For the trio of states $11f$, $R=3$, $N=0,1,2$, the ratio of the experimental widths is 2.91(59) to 2.05(31) to 1, which agrees with the theoretical ratio 2.60 to 1.81 to 1. The theory accurately predicts the n, R, and N dependence of $v=1$ H_2 autoionization rates, within experimental uncertainty.

TABLE II. A list of nf Rydberg levels observed, showing the measured natural width of the transition from $3d$ intermediate states, width expected from the theoretically predicted autoionization rates, the autoionization rate derived from the measured width, the ratio of measured width to predicted width, and the difference between experimental width and theoretical width in units of the measured standard deviation. All levels are $v=1$. An even R indicates para-H_2 and an odd R indicates ortho-H_2.

Rydberg state	Measured width (MHz)	Predicted width (MHz)	Measured rate (10^7 s^{-1})	Ratio: $\frac{\text{experiment}}{\text{theory}}$	(Experiment)-(Theory) (units of experimental σ)
$11f$ $R=0$ $N=3$[a]	221(11)	236	139(7)	0.9	−1.4
$12f$ $R=0$ $N=3$	197(10)	183	124(6)	1.1	+1.4
$13f$ $R=0$ $N=3$	160(16)	145	101(10)	1.1	+0.9
$14f$ $R=0$ $N=3$	110(14)	116	69(9)	0.9	−0.4
$15f$ $R=0$ $N=3$[a]	131(10)	95	82(6)	1.4	+3.6
$16f$ $R=0$ $N=3$	99(13)	78	62(8)	1.3	+1.6
$17f$ $R=0$ $N=3$	80(11)	65	50(7)	1.2	+1.4
$18f$ $R=0$ $N=3$	65(13)	55	41(8)	1.2	+0.8
$19f$ $R=0$ $N=3$	56(16)	47	35(10)	1.2	+0.6
$20f$ $R=0$ $N=3$	38(20)	40	24(13)	1.0	−0.1
$11f$ $R=2$ $N=2$	126(16)	146	79(10)	0.9	−1.3
$11f$ $R=2$ $N=3$[a]	200(25)	232	126(16)	0.9	−1.3
$11f$ $R=1$ $N=2$	297(16)	301	187(10)	1.0	−0.3
$12f$ $R=1$ $N=2$	229(10)	234	144(6)	1.0	−0.5
$13f$ $R=1$ $N=2$[a]	1500(500)	185	942(314)	8.1	+2.6
$14f$ $R=1$ $N=2$	159(14)	149	100(9)	1.1	+0.7
$15f$ $R=1$ $N=2$[a]	81(19)	121	51(12)	0.7	−2.1
$16f$ $R=1$ $N=2$	113(16)	100	71(10)	1.1	+0.8
$17f$ $R=1$ $N=2$	141(13)	84	89(8)	1.7	+4.4
$18f$ $R=1$ $N=2$	85(21)	71	53(13)	1.2	+0.7
$21f$ $R=1$ $N=2$	66(16)	45	41(10)	1.5	+1.3
$10f$ $R=3$ $N=0$	835(181)	641	525(114)	1.3	+1.1
$10f$ $R=3$ $N=1$	463(50)	447	291(31)	1.0	+0.3
$10f$ $R=3$ $N=2$	301(17)	248	189(11)	1.2	+3.1
$11f$ $R=3$ $N=0$[a]	535(80)	489	336(50)	1.1	+0.6
$11f$ $R=3$ $N=1$[a]	378(24)	341	238(15)	1.1	+1.5
$11f$ $R=3$ $N=2$	184(25)	188	116(16)	1.0	−0.2
$12f$ $R=3$ $N=1$	282(61)	266	177(38)	1.1	+0.3
$12f$ $R=3$ $N=2$[a]	201(18)	147	126(11)	1.4	+3.0
$13f$ $R=3$ $N=1$	250(77)	210	157(48)	1.2	+0.5
$22f$ $R=1$ $N=3$	62(26)	18	39(16)	3.4	+1.7
$15f$ $R=2$ $N=3$	105(12)	94	66(8)	1.1	+0.9
$15f$ $R=2$ $N=4$	87(17)	66	55(11)	1.3	+1.2
$20f$ $R=2$ $N=4$	44(21)	28	28(13)	1.6	+0.8
$15f$ $R=4$ $N=3$	100(18)	64	63(11)	1.6	+2.0

[a]Anomalous levels, which have an unusually large width, or an unusually large second-order correction to the energy $|E^{(2)}_{\text{quad,pol}}|$, or both, indicating the presence of nearby perturbing levels which the theory does not take into account. See Table V for a listing of the second-order energy-level correction $E^{(2)}_{\text{quad,pol}}$ for all levels.

TABLE III. A complete list of the measured energy intervals between some metastable $2p$ levels and some $3d$ intermediate levels. We measured transitions to nf Rydberg states from the first four of these $3d$ levels. All levels are $v=1$.

Transition	Interval (cm^{-1})
$(3d)^3\Sigma\, N=2\, J=3\leftarrow(2p)^3\Pi_u N=2\, J=3$ (para)	16 515.5066(20)
$(3d)^3\Sigma\, N=1\, J=2\leftarrow(2p)^3\Pi_u N=1\, J=2$ (ortho)	16 603.2649(20)
$(3d)^3\Pi\, N=2\, J=3\leftarrow(2p)^3\Pi_u N=1\, J=2$ (ortho)	16 978.5642(20)
$(3d)^3\Pi\, N=3\, J=4\leftarrow(2p)^3\Pi_u N=2\, J=3$ (para)	16 988.8851(20)
$(3d)^3\Delta\, N=3\, J=4\leftarrow(2p)^3\Pi_u N=3\, J=4$ (ortho)	17 357.7078(40)
$(3d)^3\Pi\, N=4\, J=5\leftarrow(2p)^3\Pi_u N=3\, J=4$ (ortho)	16 990.7219(20)
$(3d)^3\Pi\, N=1\, J=2\leftarrow(2p)^3\Pi_u N=1\, J=2$ (ortho)	16 988.6540(20)
$(3d)^3\Pi\, N=6\, J=7\leftarrow(2p)^3\Pi_u N=5\, J=6$ (ortho)	16 976.9749(30)
$(3d)^3\Sigma\, N=3\, J=4\leftarrow(2p)^3\Pi_u N=3\, J=4$ (ortho)	16 413.4156(50)

The Rydberg states of H_2 might also decay via channels other than autoionization. Other decay modes would broaden the lines if the rates were on the order of or larger than the autoionization rate of approximately $10^9\ s^{-1}$. No evidence has been reported for predissociation in the triplet nf, $v=1$ states we have measured. Berry and Nielsen[50] have calculated that predissociation will occur at a rate orders of magnitude slower than autoionization for the high n, $v=1$ Rydberg states we study. The radiative decay rate is expected to be roughly the same as that of a Rydberg H atom, and is about three orders of magnitude smaller than the autoionization rates of Rydberg H_2 when $L=3$. The good agreement between the measured rates and the results of the autoionization calculation strongly indicates that autoionization is the only significant decay process occurring in the nf, $v=1$ Rydberg states we have studied.

B. Line positions

As described in Sec. III, we tuned the lasers to the peaks of their transitions and used the wave meter to make 50 or more measurements of the wavelength. This homemade wave meter[46–48] interpolated the fringes recorded at the beginning and end of the retromirror travel, and proved much more precise than commercially available ones. A typical histogram of the wave meter data is shown in Fig. 11. The standard deviation of the wave meter data, about 0.0005 cm^{-1}, was very small, and since it took only 5 s to obtain each datum, the statistical uncertainty could have been made even smaller by increasing the number of readings. Unfortunately, systematic uncertainties increase this uncertainty by a factor of 4. The data in the histogram in Fig. 11 were taken within about 5 min. Data taken on different days measuring the same H_2 line shifted by apparently random amounts ranging from -0.002 to $+0.002$ cm^{-1}. Since we corrected for changes in room temperature and pressure, it appears that shifts in the optical alignment of the wave meter caused this uncertainty, which is the dominant contribution to the uncertainty of our transition frequency measurements. A much smaller systematic uncertainty was the frequency of the He-Ne reference laser,

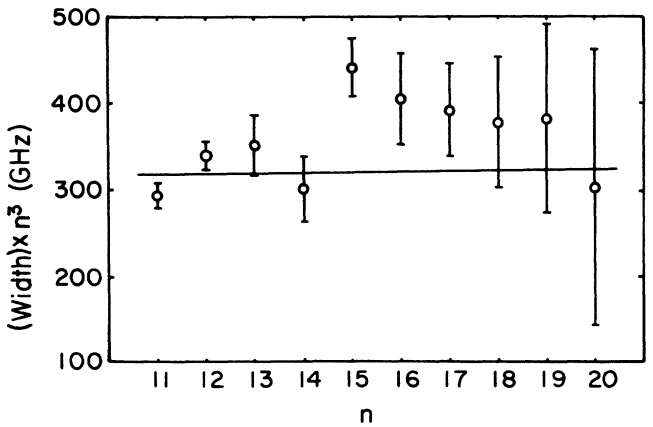

FIG. 9. Graph of width due to autoionization scaled by multiplying by n^3 vs n. This shows the scaled widths (and scaled experimental uncertainties) of the Rydberg levels $n=11$–20, $L=3$, $v=1$, $R=0$, and $N=3$.

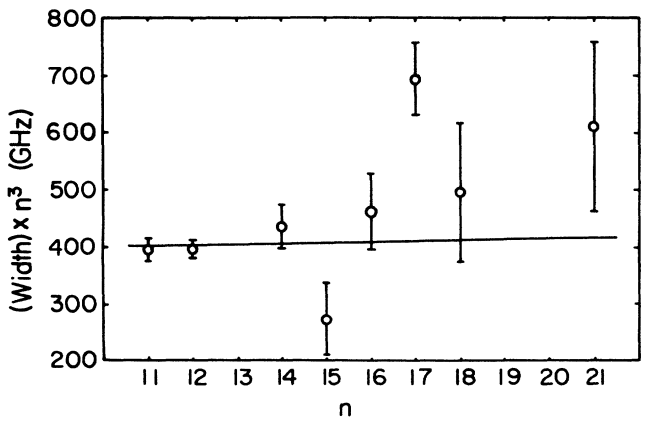

FIG. 10. Graph of width due to autoionization scaled by multiplying by n^3 vs n. This shows the scaled widths (and scaled experimental uncertainties) of the Rydberg levels $n=11$–21, $L=3$, $v=1$, $R=1$, and $N=2$.

known to ± 0.0003 cm^{-1}. All other known systematic uncertainties are insignificant.

The discussion of spin splitting of the lines in Sec. IV A applies here as well. We always measured the transition frequencies of the tops of the peaks of the lines and did not apply any corrections for asymmetry arising from unresolved structure. Seventy percent or more of the intensity (for the Rydberg states) is expected to be in the tran-

TABLE IV. A complete list of nf Rydberg levels showing the measured and theoretical intervals between nf Rydberg and intermediate $3d$ levels, and the difference $\mathcal{D}(n)$ between the measured and theoretical intervals. All levels are $v=1$. An even R indicates para-H_2 and an odd R indicates ortho-H_2.

Rydberg level	Measured interval from $3d$ level (cm^{-1})	Theoretical interval from $3d$ level (cm^{-1})	$\mathcal{D}(n)$=(experiment) −(theory) (cm^{-1})
$(2p)^3\Pi_u N=2\rightarrow(3d)^3\Sigma N=2\rightarrow$			
$11f$ $R=0$ $N=3$[b]	11 790.2600(20)	11 790.2607	−0.0007
$12f$ $R=0$ $N=3$	11 935.0011(20)	11 935.0040	−0.0029
$13f$ $R=0$ $N=3$	12 047.9583(20)	12 047.9687	−0.0104
$14f$ $R=0$ $N=3$	12 137.5346(20)	12 137.5446	−0.0100
$15f$ $R=0$ $N=3$[b]	12 209.5122(20)	12 209.4894	+0.0228
$16f$ $R=0$ $N=3$	12 268.8488(20)	12 268.8503	−0.0015
$17f$ $R=0$ $N=3$	12 317.8642(20)	12 317.8707	−0.0065
$18f$ $R=0$ $N=3$	12 358.8646(20)	12 358.8729	−0.0083
$19f$ $R=0$ $N=3$	12 393.6333(20)	12 393.6372	−0.0039
$20f$ $R=0$ $N=3$	12 423.2647(20)	12 423.2662	−0.0015
$11f$ $R=2$ $N=2$	11 954.7202(20)	11 954.6663	+0.0539
$11f$ $R=2$ $N=3$[b]	11 956.1569(20)	11 956.1931	−0.0362
$(2p)^3\Pi_u N=1\rightarrow(3d)^3\Sigma N=1\rightarrow$			
$11f$ $R=1$ $N=2$	11 871.2189(20)	11 871.2173	+0.0016
$12f$ $R=1$ $N=2$	12 016.5416(20)	12 016.5367	+0.0049
$13f$ $R=1$ $N=2$[a]	12 129.5448(20)	12 129.5773	−0.0325
$14f$ $R=1$ $N=2$	12 219.3136(20)	12 219.3016	+0.0120
$15f$ $R=1$ $N=2$[b]	12 291.8741(20)	12 291.9780	−0.1039
$16f$ $R=1$ $N=2$	12 350.8649(20)	12 350.8496	+0.0153
$17f$ $R=1$ $N=2$	12 399.8915(20)	12 399.8750	+0.0165
$18f$ $R=1$ $N=2$	12 441.0286(20)	12 441.0108	+0.0178
$21f$ $R=1$ $N=2$	12 531.0540(20)	12 531.0328	+0.0212
$10f$ $R=3$ $N=0$[c]	11 952.1749(30)	11 952.4001	−0.2252
$10f$ $R=3$ $N=1$[c]	11 953.1048(20)	11 953.1363	−0.0315
$10f$ $R=3$ $N=2$[c]	11 954.5033(20)	11 954.4363	+0.0670
$11f$ $R=3$ $N=0$[b,c]	12 143.8686(20)	12 143.9962	−0.1276
$11f$ $R=3$ $N=1$[b,c]	12 144.4831(20)	12 144.5086	−0.0255
$11f$ $R=3$ $N=2$[c]	12 145.4910(20)	12 145.4442	+0.0468
$12f$ $R=3$ $N=1$[c]	12 289.8841(20)	12 289.8514	+0.0327
$12f$ $R=3$ $N=2$[b,c]	12 290.4469(20)	12 290.2725	+0.1744
$13f$ $R=3$ $N=1$[c]	12 403.0140(20)	12 403.0285	−0.0145
$(2p)^3\Pi_u N=1\rightarrow(3d)^3\Pi N=2\rightarrow$			
$22f$ $R=1$ $N=3$	12 178.2742(20)	12 178.2388	+0.0354
$(2p)^3\Pi_u N=2\rightarrow(3d)^3\Pi N=3\rightarrow$			
$15f$ $R=2$ $N=3$	11 901.7673(20)	11 901.7922	−0.0249
$15f$ $R=2$ $N=4$	11 901.9165(20)	11 901.9047	+0.0118
$20f$ $R=2$ $N=4$	12 115.1003(30)	12 115.0961	+0.0042

[a,b]Anomalous levels, which have (a) an unusually large width or (b) an unusually large second-order correction to the energy $|E^{(2)}_{\text{quad,pol}}|$, indicating the presence of nearby perturbing levels which the theory does not take into account. See Table V for a listing of the second-order energy-level correction $E^{(2)}_{\text{quad,pol}}$ for these levels.

[c]These theoretical intervals are based on an extrapolation to $R=3$ of Bishop and Cheung's (Ref. 22) results for $E(v,R)$.

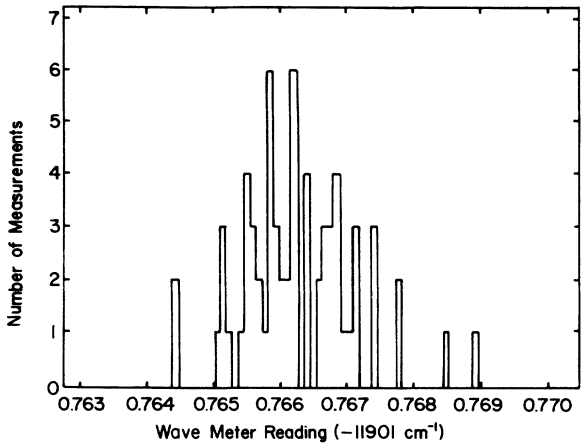

FIG. 11. A typical histogram of one set of wave meter measurements of a transition from an intermediate to Rydberg state. This particular measurement was of the $15f, v=1$, $R=2, N=3 \leftarrow (3d)^3\Pi, v=1, N=3$ transition.

sition to J_{max}. Since the splitting for different values of J is approximately 20 MHz or less, significantly less than our experimental uncertainty for the transition frequencies, any possible shifts in the line center caused by the spin structure of transitions would be less than the experimental uncertainty of 60 MHz.

For some wide weak lines, it was difficult to set the ir laser to the exact top of the peak to a precision of 0.002 cm^{-1} (60 MHz). Consequently, the transition frequencies of these lines are less precise, depending on how weak and wide they were.

Table III shows the intervals measured for transitions from the $2p$ metastable states to the $3d$ intermediate states. Table IV presents the intervals measured for transitions from the $3d$ states to the nf Rydberg states.

C. Ionization potentials

Column 3 of Table IV shows the theoretical values for the $\Delta E(nf \leftarrow 3d)$ intervals, which are calculated according to the formula (see Fig. 12)

$$\Delta E(nf \leftarrow 3d) = V_{ion}(H_2) - \mathcal{R}/n^2 + E_{quad,pol} + E(v,R) - \Delta E(2p \leftarrow X) - \Delta E(3d \leftarrow 2p) \ . \quad (2)$$

In Eq. (2) X refers to the singlet ground state ($N=0$ for para, $N=1$ for ortho) of H_2, $2p$ refers to the metastable state, $3d$ refers to the intermediate state, and nf refers to the Rydberg state. Each of the labels X, $2p$, $3d$, and nf is shorthand for the full complement of appropriate quantum numbers necessary to identify the level. $V_{ion}(H_2)$ is the ionization potential of the hydrogen molecule in its ground state. $\mathcal{R}(H_2) = 109\,707.4496\ cm^{-1}$ is the reduced mass Rydberg constant for a nuclear (core, in this case) mass of two protons and one electron. $E_{quad,pol}$ is the sum $E^{(1)}_{quad,pol} + E^{(2)}_{quad,pol}$, where $E^{(1)}_{quad,pol} = \langle \mathcal{H}_{quad} \rangle + \langle \mathcal{H}_{pol} \rangle$ is the first-order result of the polarizability-quadrupole moment long-range interaction model of Ref. 18, and $E^{(2)}_{quad,pol}$ is the second-order result.[36] $E(v,R)$ are the vibrational and rotational energy levels of the H_2^+ core, taken from the calculations of Bishop and Cheung,[22] as shown in Table I. They estimate their uncertainty to be 0.002 cm^{-1}. The right-hand side of this equation contains several experimental inputs, which are the two ΔE's and the $V_{ion}(H_2)$. The value of $V_{ion}(H_2)$ used was the recent and very precise result of McCormack *et al.*,[38] who measured and analyzed the singlet np Rydberg states to obtain a value of $V_{ion}(H_2) = 124\,417.524(15)\ cm^{-1}$. We measured $\Delta E(3d \leftarrow 2p)$, as reported in Table III, to a precision of 0.002 cm^{-1}. $\Delta E(2p \leftarrow X)$ to our knowledge has never been measured directly or calculated with an uncertainty approaching 0.01 cm^{-1}. If we had used Dieke's[9,10] original values for $\Delta E(2p \leftarrow X)$, as corrected by Miller and Freund,[11]

$$\Delta E[(2p)^3\Pi_u v=1\, N=2 \leftarrow X(\text{para})] = 97\,395.57\ cm^{-1} \ ,$$

$$\Delta E[(2p)^3\Pi_u v=1\, N=1 \leftarrow X(\text{ortho})] = 97\,280.54\ cm^{-1} \ ,$$

in Eq. (2), the difference $\mathcal{D}$ (experiment-theory) in column 4 of Table IV would have been an approximately constant nonzero value of about $+0.124\ cm^{-1}$. The approximately constant nonzero value of this difference $\mathcal{D}$ as a function of n indicates that the long-range model is quite successful but that Dieke's initial values of $\Delta E(2p \leftarrow X)$ are incorrect by a constant amount. The scatter of these differences $\mathcal{D}$ around their average value as n changes is approximately 0.02 cm^{-1}. Since $\mathcal{R}/n^2$ and $E_{quad,pol}$ are the only n-dependent terms in Eq. (2), and the uncertainty of $\mathcal{R}/n^2$ is only a few parts in 10^{10}, the scatter in $\mathcal{D}$ must be due to $E_{quad,pol}$. We estimate the systematic uncertainty in $E_{quad,pol}$ to be 0.020 cm^{-1}. The value of $E_{quad,pol}$ is typically about $-1\ cm^{-1}$.

The ionization potential of the $(2p)^3\Pi_u$ states, $V_{ion}(2p)$, is given by (see Fig. 12)

$$V_{ion}(2p) = \Delta E(3d \leftarrow 2p) + \Delta E(nf \leftarrow 3d) + \mathcal{R}(H_2)/n^2 - E(v,R) - E_{quad,pol} \ . \quad (3)$$

Each choice of nf state and $3d$ state gives a slightly different value of $V_{ion}(2p)$, but of course the result of Eq. (3) ought to be constant for a given $2p$ state. We average all the $V_{ion}(2p)$'s obtained from excitations from a given $2p$ state to nonanomalous nf states (see Sec. IV D for an explanation of anomalous states), giving the results

$$V_{ion}[(2p)^3\Pi_u v=1\, N=2\, J=3\, F=3(\text{para})] = 27\,022.088(20)\ cm^{-1} \ ,$$

$$V_{ion}[(2p)^3\Pi_u v=1\, N=1\, J=2\, F=3(\text{ortho})] = 27\,137.099(20)\ cm^{-1} \ .$$

The uncertainties are given by the uncertainties of each of the terms of Eq. (3), which are, respectively (in cm^{-1}), 0.002, 0.002, 0, 0.002, and 0.020. The sum in quadrature is 0.020 cm^{-1}.

$\Delta E(2p \leftarrow X)$ for each of the metastable $2p$ levels examined is given by

$$\Delta E(2p \leftarrow X) = V_{\text{ion}}(H_2) - V_{\text{ion}}(2p) \ , \tag{4}$$

using the above average $V_{\text{ion}}(2p)$'s. The results are

$$\Delta E[(2p)^3\Pi_u v=1\, N=2\, J=3\, F=3 \leftarrow X(\text{para})] = 97\,395.436(25)\ \text{cm}^{-1} \ ,$$

$$\Delta E[(2p)^3\Pi_u v=1\, N=1\, J=2\, F=3 \leftarrow X(\text{ortho})] = 97\,280.425(25)\ \text{cm}^{-1} \ .$$

The uncertainties are given by the uncertainties of each of the terms of Eq. (4), which are, respectively (in cm^{-1}), 0.015 and 0.020. The sum in quadrature is 0.025 cm^{-1}.

Eyler, Short, and Pipkin[36] measured the above $V_{\text{ion}}(2p)$'s and found $V_{\text{ion}}[2p(\text{para})]$ to be 27 022.01(2) cm^{-1}, which is more than three standard deviations away from our result. This discrepancy was traced to their use of a value for

$$\Delta E[(3d)^3\Sigma, v=1, N=2 \leftarrow (2p)^3\Pi, v=1, N=2]$$

of 16 515.46(1) cm^{-1}, taken from Ref. 13. As shown in Table III, we measured the same transition to be at 16 515.5066(20) cm^{-1}. Eyler, Short, and Pipkin's reported difference of 0.03 cm^{-1} between the ionization potentials of para-H_2 and ortho-H_2 from the ground state is also brought to the expected value of zero within their experimental uncertainty by replacing 16 515.46 with 16 515.5066 in their analysis. Our value for $V_{\text{ion}}[2p$ (ortho)] is the same as in Ref. 36, within their quoted uncertainty.

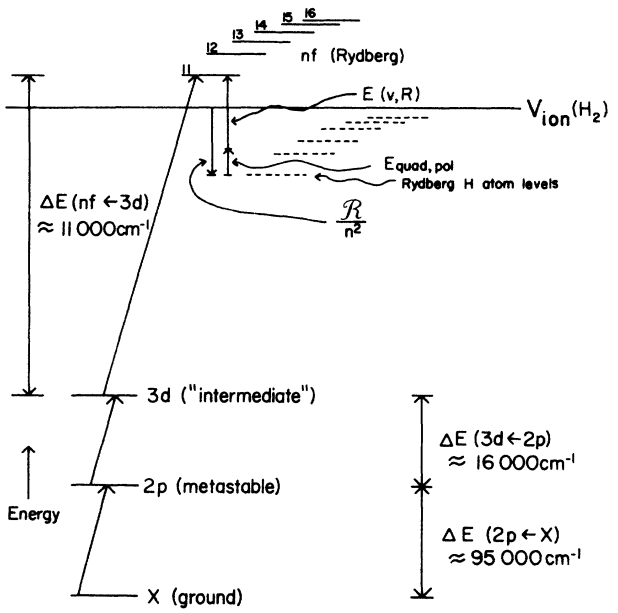

FIG. 12. Excitation scheme showing the details of the energy-level shifts from unperturbed Rydberg H atom levels caused by the H_2^+ molecular core. The Rydberg series of states above the $V_{\text{ion}}(H_2)$ level are the actual Rydberg states to which we observe transitions. The energy levels of the actual states are calculated by adding two corrections to the Rydberg H atom energy levels given by $V_{\text{ion}} - \mathcal{R}/n^2$. $E(v,R)$ is the vibrational and rotational energy of the core, and $E_{\text{quad,pol}}$ is the correction due to the long-range model. $E_{\text{quad,pol}}$ is shown as a positive quantity in the drawing for clarity, but in fact for all the H_2 states we examined, it is a negative quantity. This diagram is not to scale vertically.

D. Anomalous transitions

Certain transitions (marked in Tables II, IV, and V) had unusually large values of $|E^{(2)}_{\text{quad,pol}}|$ leading to either anomalously large $\mathcal{D}(n)$, or anomalously wide or narrow widths. In each of these cases there was another state, possibly with a much faster autoionization rate, very close in energy to the anomalous state. The two states mixed with and perturbed each other.[1] Table V lists the

TABLE V. Second-order energy corrections $E^{(2)}_{\text{quad,pol}}$ to Rydberg levels. If the correction is large and the level is perturbed, the level is marked with an × in the third column. All levels are $v=1$.

Rydberg state	$E^{(2)}_{\text{quad,pol}}$ (cm^{-1})	Perturbed state
$11f\ R=0\ N=3$	0.2128	×
$12f\ R=0\ N=3$	−0.0825	
$13f\ R=0\ N=3$	0.0207	
$14f\ R=0\ N=3$	0.0532	
$15f\ R=0\ N=3$	−0.2350	×
$16f\ R=0\ N=3$	0.0131	
$17f\ R=0\ N=3$	0.0455	
$18f\ R=0\ N=3$	−0.0023	
$19f\ R=0\ N=3$	0.0233	
$20f\ R=0\ N=3$	−0.0056	
$11f\ R=2\ N=2$	0.0517	
$11f\ R=2\ N=3$	0.2220	×
$11f\ R=1\ N=2$	0.0864	
$12f\ R=1\ N=2$	0.0609	
$13f\ R=1\ N=2$	0.0205	×
$14f\ R=1\ N=2$	0.0401	
$15f\ R=1\ N=2$	0.3623	×
$16f\ R=1\ N=2$	0.0282	
$17f\ R=1\ N=2$	−0.0068	
$18f\ R=1\ N=2$	0.0220	
$21f\ R=1\ N=2$	0.0125	
$10f\ R=3\ N=0$	0.0354	
$10f\ R=3\ N=1$	0.0230	
$10f\ R=3\ N=2$	0.0254	
$11f\ R=3\ N=0$	0.1637	×
$11f\ R=3\ N=1$	0.1132	×
$11f\ R=3\ N=2$	0.0731	
$12f\ R=3\ N=1$	0.0260	
$12f\ R=3\ N=2$	−0.3049	×
$13f\ R=3\ N=1$	0.0611	
$22f\ R=1\ N=3$	−0.0036	
$15f\ R=2\ N=3$	0.0484	
$15f\ R=2\ N=4$	0.0348	
$20f\ R=2\ N=4$	−0.0502	
$15f\ R=4\ N=3$	−0.0158	

Rydberg states we measured and shows all the corresponding values of $E^{(2)}_{\text{quad,pol}}$. If $|E^{(2)}_{\text{quad,pol}}|$ is large (greater than about 0.1 cm^{-1}), or if the state is drastically widened and distorted, Table V shows an X in the third column. A more precise, higher-order calculation that treats strong localized perturbations would be necessary to predict the positions of these perturbed levels, so these transitions were not used in the calculations of the average values of $V_{\text{ion}}(2p)$ and $\Delta E(2p \leftarrow X)$ in Sec. IV C.

V. CONCLUSION

We have measured the autoionization rates and transition energies of a variety of triplet nf, $v=1$ Rydberg states of H_2, using narrow linewidth single-mode cw dye lasers crossed with a molecular beam. Our autoionization rate data agree satisfactorily with the predictions of the long-range model,[1,19] which are based on the interaction of the Rydberg electron with the polarizability and quadrupole moment of the H_2^+ core. Our measurements of the transition frequencies are accurate to 0.002 cm^{-1}. The predicted values of the transition frequencies[18,19] do not agree well with the measurements. The effects of higher-order interactions, spin, and close-lying perturbing states need to be added to the theory in order to obtain energy-level predictions to the experimental accuracy of 0.002 cm^{-1}. Possibly a multichannel quantum-defect theory can be used to obtain more accurate predictions. Additionally, we have found the absolute energy levels of two triplet $c(2p)^3\Pi_u$, $v=1$ metastable states of H_2 relative to the ionization limit to an accuracy of 0.020 cm^{-1}, and relative to the singlet ground state to an accuracy of 0.025 cm^{-1}. This links the singlet and triplet manifolds of H_2 with very high precision.

Our values of $\Delta E(2p \leftarrow X)$ for two particular $2p$ triplet states provide a correction to two numbers contained on p. E8 of Dieke's tables.[9] One must bear in mind that Dieke's energy levels were derived from the weighted average of the fine-structure components. We measured the intervals between specific fine-structure components of the H_2 states. For para-H_2, the center of gravity of the fine-structure energy levels is 0.067 cm^{-1} away[13] from the measured $N=2$, $J=3$ fine-structure component. For ortho-H_2, the center of gravity of the fine structure energy levels is 0.058 cm^{-1} away[13] from the measured $N=1$, $J=2$, $F=3$ fine-structure component. We have added these center-of-gravity shifts relative to the specific fine-structure components to our values of $\Delta E(2p \leftarrow X)$ in order to compare our numbers directly with Dieke's values of $\Delta E(2p \leftarrow X)$. We find that the shift needed to make Dieke's triplet term values correct is $-149.662(25)$ cm^{-1}. This is an update of the Miller and Freund correction[11] of -149.6 cm^{-1}. The accuracy of this updated correction for all of the rest of the triplet states in Dieke's table depends on the accuracy of Dieke's measurements within the triplet manifold.

ACKNOWLEDGMENTS

This research was supported in part by National Science Foundation Grant No. PHY-8704527. Calculations were supported in part by National Science Foundation Grant No. PHY-8717051. One of us (M.D.L.) thanks Stone & Webster Corp. for partial support; J.R.L. would like to acknowledge support from Bell Laboratories; A.W.K. would like to acknowledge support from the Shell Foundation. We thank W. Lichten for use of the I_2-stabilized laser.

[1] E. E. Eyler, Phys. Rev. A **34**, 2881 (1986).
[2] P. M. Dehmer and W. A. Chupka, J. Chem. Phys. **65**, 2243 (1976).
[3] P. M. Dehmer and W. A. Chupka, J. Chem. Phys. **66**, 1972 (1977).
[4] E. E. Eyler, W. A. Chupka, S. D. Colson, and D. T. Biernacki, Chem. Phys. Lett. **119**, 177 (1985).
[5] D. T. Biernacki, S. D. Colson, and E. E. Eyler, J. Chem. Phys. **88**, 2099 (1988); **89**, 2599 (1988).
[6] O. W. Richardson and P. M. Davidson, Proc. R. Soc. London **142**, 40 (1933).
[7] E. W. Foster and O. W. Richardson, Proc. R. Soc. London **189**, 149 (1947); **189**, 175 (1947).
[8] O. W. Richardson, *Molecular Hydrogen and Its Spectrum* (Yale University Press, New Haven, CT, 1934).
[9] Crosswhite's compendium of Dieke's results: H. M. Crosswhite, *The Hydrogen Molecule Wavelength Tables of Gerhard Heinrich Dieke* (Wiley-Interscience, New York, 1972).
[10] G. H. Dieke, J. Mol. Spectrosc. **2**, 494 (1958).
[11] T. A. Miller and R. S. Freund, J. Chem. Phys. **61**, 2160 (1974).
[12] W. Lichten, Phys. Rev. **120**, 848 (1960); **126**, 1020 (1962).
[13] T. R. Wik, Ph.D. thesis, Yale University, 1977 (unpublished); W. Lichten and T. Wik, J. Chem. Phys. **69**, 5428 (1978); W. Lichten, T. Wik, and T. A. Miller, *ibid.* **71**, 2441 (1979).
[14] Miller and Freund have published at least 20 papers throughout the 1970s on H_2. Some examples are T. A. Miller and R. S. Freund, J. Chem. Phys. **58**, 2345 (1973); **59**, 4093 (1973); R. S. Freund, T. A. Miller, R. Jost, and M. Lombardi, *ibid.* **68**, 1683 (1978); T. A. Miller, *ibid.* **59**, 4078 (1973).
[15] A. Norman Jette and T. A. Miller, Chem. Phys. Lett. **29**, 547 (1974).
[16] Ch. Jungen and E. Meischer, Can. J. Phys. **47**, 1769 (1969).
[17] G. Herzberg and Ch. Jungen, J. Chem. Phys. **77**, 5876 (1982).
[18] E. E. Eyler and F. M. Pipkin, Phys. Rev. A **27**, 2462 (1983); **29**, 1588(E) (1984).
[19] E. E. Eyler, Ph.D. thesis, Harvard University, 1982 (unpublished).
[20] W. G. Sturrus, P. E. Sobol, and S. R. Lundeen, Phys. Rev. Lett. **54**, 792 (1985); W. G. Sturrus, E. A. Hessels, and S. R. Lundeen, *ibid.* **57**, 1863 (1986); W. G. Sturrus, E. A. Hessels, P. W. Arcuni, and S. R. Lundeen, Phys. Rev. A **38**, 135 (1988); Phys. Rev. Lett. **61**, 2320 (1988); E. A. Hessels, W. G. Sturrus, and S. R. Lundeen, Phys. Rev. A **38**, 4574 (1988).
[21] D. M. Bishop and L. M. Cheung, J. Phys. B **11**, 3133 (1978).
[22] D. M. Bishop and L. M. Cheung, Phys. Rev. A **16**, 640 (1977).
[23] G. Karl, B. Nickel, J. D. Poll, and L. Wolniewicz, Phys. Rev. Lett. **34**, 1302 (1975).
[24] A. Russek, M. R. Patterson, and R. L. Becker, Phys. Rev. **167**, 17 (1968).
[25] G. Herzberg and Ch. Jungen, J. Mol. Spectrosc. **41**, 425 (1972).
[26] C. H. Greene and Ch. Jungen, in *Advances in Atomic and Molecular Physics*, edited by D. Bates and B. Bederson

(Academic, New York, 1985), Vol. 21, pp. 51–123, and references therein.

[27]Ch. Jungen and D. Dill, J. Chem. Phys. **73**, 3338 (1980); Ch. Jungen and O. Atabek, *ibid.* **66**, 5584 (1970); Ch. Jungen, Phys. Rev. Lett. **53**, 2394 (1984); M. Raoult and Ch. Jungen, J. Chem. Phys. **74**, 3388 (1981).

[28]Ch. Jungen, I. Dabrowski, G. Herzberg, and D. J. W. Kendall, J. Chem. Phys. **91**, 3926 (1989).

[29]G. Herzberg, *Molecular Spectra and Molecular Structure: I. Spectra of Diatomic Molecules,* 2nd ed. (Van Nostrand, Princeton, NJ, 1950).

[30]M. Krauss, Natl. Bur. Stand. (U.S.) Tech. Note 438 (U.S. GPO, Washington, D.C., 1967).

[31]T. E. Sharp, At. Data **2**, 119 (1971).

[32]G. Herzberg, Commentat. Pontif. Acad. Sci. **2**, 1 (1972).

[33]D. M. Bishop and L. M. Cheung, Mol. Phys. **36**, 501 (1978).

[34]R. S. Freund, in *Rydberg States of Atoms and Molecules,* edited by R. F. Stebbings and F. B. Dunning (Cambridge University Press, New York, 1983), pp. 355–392.

[35]E. E. Eyler and F. M. Pipkin, Phys. Rev. Lett. **47**, 1270 (1981); J. Chem. Phys. **77**, 5315 (1982).

[36]E. E. Eyler, R. C. Short, and F. M. Pipkin, Phys. Rev. Lett. **56**, 2602 (1986).

[37]E. E. Eyler, J. M. Gilligan, E. McCormack, A. Nussenzweig, and E. Pollack, Phys. Rev. A **36**, 3486 (1987).

[38]E. McCormack, J. M. Gilligan, C. Cornaggia, and E. E. Eyler, Phys. Rev. A **39**, 2260 (1989).

[39]G. Hunter, A. W. Yau, and H. O. Pritchard, At. Data Nucl. Data Tables **14**, 11 (1974).

[40]J. L. Hunt, J. D. Poll, and L. Wolniewicz, Can. J. Phys. **62**, 1719 (1984).

[41]J. T. Hougen, *The Calculation of Rotational Energy Levels and Rotational Line Intensities in Diatomic Molecules,* Natl. Bur. Stand. (U.S.) Monograph 115 (U.S. GPO, Washington D.C., 1970).

[42]For homonuclear molecules such as H_2 there is no permanent dipole moment, thus $\mathcal{H}_{\text{dipole}}=0$.

[43]The "slit" was actually formed from a slit cut into the Cu rod, separated by a gap from another slit in a block of Cu held in alignment with the first slit. These slits were cut by electric discharge machining.

[44]S. Gerstenkorn and P. Luc, *Atlas du Spectre d'Absorption de la Molecule d'Iode: 14 800–20 000 cm^{-1}* (CNRS, Paris, 1978). A systematic correction to this reference is described by S. Gerstenkorn and P. Luc, Rev. Phys. Appl. **14**, 791 (1979).

[45]S. Gerstenkorn, J. Verges, and G. Chevillard, *Atlas du Spectra d'Absorption de la Molecule d'Iode: 11 000 cm^{-1}–14 000 cm^{-1}* (Laboratoire Aimé-Cotton, CNRS II, Orsay, France, 1982).

[46]J. L. Hall and S. A. Lee, Appl. Phys. Lett. **29**, 367 (1976).

[47]A. W. Kam, J. R. Lawall, M. D. Lindsay, F. M. Pipkin, R. C. Short, and P. Zhao, Phys. Rev. A **40**, 1279 (1989).

[48]T. Baer, R. V. Kowalski, and J. L. Hall, Appl. Opt. **19**, 3173 (1980).

[49]W. H. Press, B. P. Flannery, S. A. Teukolsky, W. T. Vetterling, *Numerical Recipes: The Art of Scientific Computing* (Cambridge University Press, New York, 1986), p. 523.

[50]R. S. Berry and S. E. Nielsen, Phys. Rev. A **1**, 395 (1970).